Amino Acids (2025) 57:27
https://doi.org/10.1007/s00726-025-03456-3

ORIGINAL ARTICLE

Targeting LAT1 with JPH203 to reduce TNBC proliferation and reshape suppressive immune microenvironment by blocking essential amino acid uptake

Yajie Zhao[1] · Chunrui Pu[1] · Kangdong Liu[2] · Zhenzhen Liu[1]

Received: 15 March 2025 / Accepted: 28 April 2025
© The Author(s) 2025

Abstract

The competitive uptake of essential amino acids (EAAs) by breast cancer cells is associated with poor patient prognosis and the development of an immunosuppressive tumor microenvironment. L-type amino acid transporters, LAT1 (*SLC7 A5*) and LAT2 (*SLC7 A8*) are major mediators of EAAs transmembrane uptake and are overexpressed in some tumor tissues. However, the distribution and functional roles of these transporters across breast cancer subtypes have not been fully elucidated. This study aims to investigate the therapeutic potential of targeting EAA transporters, particularly LAT1, in triple-negative breast cancer (TNBC) and its role in remodeling the tumor immune microenvironment. The distribution of EAA transporters across breast cancer subtypes was analyzed using multi-omics data. The effects of LAT1 targeting on TNBC cell proliferation and EAA uptake were evaluated using *SLC7 A5* knockout and LAT1 inhibitors in vitro experiments. A 4T1-BALB/c tumor-bearing mouse model with normal immune function was constructed to investigate the effects of LAT1 targeting on tumor growth and immune microenvironment remodeling in vivo. TNBC demonstrated a strong dependence on LAT1-mediated EAAs uptake. Targeting LAT1 limited the exogenous supply of EAAs, leading to amino acid starvation, cell cycle arrest, and increased apoptosis in TNBC cells. The in vivo experiments, using a 4T1-BALB/c tumor-bearing mouse model, showed that LAT1 targeting inhibited tumor growth and remodeled the immunosuppressive tumor microenvironment. Targeting LAT1 improved PD-L1-associated immune suppression and improved the efficacy of PD-1 antibody treatment, producing synergistic anti-tumor effects. This study highlights the therapeutic potential of targeting LAT1 in TNBC, particularly in remodeling the tumor immune microenvironment. The findings provide a promising strategy for immune combination therapy in TNBC.

Keywords Breast cancer · Essential amino acid · JPH203 · Immune microenvironment

Abbreviations

TNBC	Triple-negative breast cancer
EAA	Essential amino acid
TCGA	The Cancer Genome Atlas
CCLE	Cancer Cell Line Encyclopedia
METABRIC	Molecular Taxonomy of Breast Cancer International Consortium
ICIs	Immune checkpoint inhibitors
m-IHC	Multiplex immunohistochemistry
IHC	Immunohistochemistry
AOD	Average optical density
MFI	Mean fluorescence intensity

Handling editor: S. Broer.

✉ Kangdong Liu
kdliu@zzu.edu.cn

✉ Zhenzhen Liu
zlyyliuzhenzhen0800@zzu.edu.cn

[1] Department of Breast Disease, Henan Breast Cancer Centre, The Affiliated Cancer Hospital of Zhengzhou University and Henan Cancer Hospital, Zhengzhou, China

[2] Department of Pathophysiology, School of Basic Medical Sciences, Zhengzhou University, Zhengzhou, China

Introduction

Triple-negative breast cancer (TNBC) accounts for approximately 15% of all breast cancer cases. Compared to other subtypes, TNBC is characterized by high invasiveness, poor prognosis, and resistance to endocrine therapy and anti-HER-2 therapy (Giaquinto et al. 2024). Current treatment strategies primarily rely on surgery combined with radiotherapy and chemotherapy, which, while extending patient

Published online: 17 May 2025

survival to some extent, have limited efficacy. The advent of immune checkpoint inhibitors (ICIs) has brought new hope for TNBC treatment. However, clinical studies have shown that PD-1 monotherapy provides limited disease control and survival benefits for TNBC patients. Moreover, PD-1 combined with chemotherapy benefits only a small subset of patients, falling short of expectations for immunotherapy (Nanda et al. 2016; Adams et al. 2019; Winer et al. 2021; Cortes et al. 2020). Addressing the suppression of immune effector cell function by the tumor microenvironment is important for improving immunotherapy outcomes.

Rapid proliferation is a hallmark of tumor cells. In order to meet the needs of rapid proliferation, tumor cells need to uptake substantial EAAs. In addition, the competitive uptake of EAAs by tumor cells significantly inhibits the immune response in the tumor microenvironment (Martínez-Reyes and Chandel 2021). Targeting tumor-specific metabolic pathways offers a novel approach to simultaneously inhibit tumor growth and reshape the immune microenvironment, thereby improving the efficacy of TNBC immunotherapy (Luengo et al. 2017; Dey et al. 2021). Our previous research demonstrated significantly higher levels of amino acids, particularly essential amino acids (EAAs), in breast cancer tissue compared to normal breast tissue, suggesting that breast cancer cells had increased EAA uptake. This phenomenon is associated with poor patient prognosis and the development of an immunosuppressive tumor microenvironment (Zhao et al. 2022). These findings support the hypothesis that limiting EAA uptake may provide a promising therapeutic approach for breast cancer treatment.

Due to EAAs being polar small molecules, their exogenous uptake is mediated by amino acid transporters. Among the 60 known amino acid transporters (Kandasamy et al. 2018), two main transporters facilitate EAA transmembrane transport: L-type amino acid transporter 1 (LAT1/*SLC7 A5*) and transporter 2 (LAT2/*SLC7 A8*), which are covalently associated with 4 F2 hc (CD98/*SLC3 A2*) (Kanai et al. 1998; Segawa et al. 1999). Literature reports indicate that LAT1 and LAT2 are highly expressed in some types of tumors and are associated with poor prognosis, making them promising molecular targets for cancer therapy (Wang and Holst 2015; Kaira et al. 2011; Maimaiti et al. 2020; Luo et al. 2009). Targeting LAT1 or LAT2 in vitro has been shown to inhibit the proliferation of several cancer types, including lymphoma, thyroid, and pancreatic cancers (Rosilio et al. 2015; Feng et al. 2018; Häfliger et al. 2018; Markowicz-Piasecka et al. 2020). However, the heterogeneity of EAA transporters across different tumor types results in variable therapeutic sensitivity to their inhibition. At present, the distribution characteristics and therapeutic roles of EAA transporters in breast cancer subtypes have not been fully elucidated.

This study aims to explore the therapeutic potential of targeting EAA metabolism in breast cancer, specifically focusing on its impact on the tumor immune microenvironment. This study is the first to propose the distribution differences of EAA transporters across different molecular subtypes of breast cancer, demonstrating that TNBC shows a strong dependence on the LAT1 transporter for EAA uptake. Using the LAT1 inhibitor JPH203, LAT1 was targeted to block exogenous EAA supply, inducing amino acid starvation, cell cycle arrest, and apoptosis in TNBC. Furthermore, in vivo experiments in a TNBC tumor-bearing mouse model with normal immune function confirmed the anti-tumor activity and safety of JPH203. LAT1 inhibition reshaped the immunosuppressive tumor microenvironment by mitigating PD-L1-mediated immune suppression and improved the efficacy of PD-1 antibodies. In summary, this study highlights the therapeutic value of targeting LAT1 in TNBC, offering a promising therapy approach to improve outcomes for patients with this aggressive breast cancer subtype, TNBC.

Methods

Patient sample collection and public database

RNA sequencing (RNA-seq) and metabolomics data for 49 breast cancer cell lines were obtained from the Encyclopedia of Cancer Cell Lines (CCLE). Additional data were analyzed from the Cancer Genome Atlas (TCGA; $n = 945$), the Molecular Taxonomy of Breast Cancer International Consortium (METABRIC; $n = 1559$) database (hts://www.Cbioportal. org/), and the Henan Cancer Hospital breast cancer dataset (HNCH-BC; $n = 122$). RNA-seq and metabolomics data were also collected from breast cancer tissues and matched adjacent tissues of 36 breast cancer patients treated at Henan Cancer Hospital, as well as 80 breast cancer patients'breast cancer tissue samples.

Cell lines and cell culture

Human breast cancer cell lines [MDA-MB-231(#CL-0150), HCC1937(#CL-0093), SK-BR-3(#CL-0211), BT474(#CL-0040), T47D(#CL-0228)]and a mouse breast cancer cell line [4 T1(#CL-0007)] were purchased from Pricella (Wuhan, China) and certified by the supplier. The cells were cultured in specialized media provided by Pricella and maintained at 37 °C in a humidified atmosphere containing 5% CO_2.

Total RNA extraction of and quantitative RT-PCR

Total RNA was extracted from cells using the FastPure® Cell/Tissue Total RNA Isolation Kit (Vazyme, RC101-1) according to the manufacturer's instructions. RNA quantification was performed using the HiScript® II One-Step

Table 1 The primer sequences for each gene

LAT1/*SLC7 A5*	forward 5′-CAAGGACATCTTTCCGTCATC-3′
	reverse 5′-AGCCACTTGGGCTTGTTT-3′
LAT2/*SLC7 A8*	forward 5′-AAAGGGAGTGCTGGAATG-3′
	reverse 5′-GACCATGTGAGGAGCATAA-3′
GAPDH	forward 5′-CTTTGGTATCGTGGAAGGACTC-3′
	reverse 5′-AGTAGGGCAGGGATGATGT-3′

qRT-PCR SYBR Green Kit (Vazyme, Q221-01). The qRT-PCR reaction mixture (20μL) included 5.8μL RNase-free water, 10μL 2 × One Step SYBR Green Mix, 1μL One Step SYBR Green Enzyme Mix, 0.4μL 50 × ROX Reference Dye I, 0.4μL each primer (10 μM), and 2μL template RNA. The amplification process involved an initial step at 50 °C for 3 min, 95 °C for 30 s, followed by 40 cycles of 95 °C for 10 s and 60 °C for 30 s. The default melting curve steps were run on an ABI™ 7300 Real-Time PCR System (Applied Biosystems, Foster City, CA, USA). Gene expression levels were normalized to GAPDH and calculated using the $2^{-\Delta\Delta Ct}$ method. The primer sequences for each gene are shown in Table 1.

Establishment of *SLC7 A5* knockdown stable cell lines

A lentiviral short hairpin RNA (shRNA) vector targeting *SLC7 A5* was obtained from GeneChem (Shanghai, China). Lentiviral particles were produced by co-transfecting the shRNA vector (shSLC7 A5-1, TRCN0000043008; shSLC7 A5-2, TRCN0000043010) with packaging plasmids into HEK293 T cells. To establish stable *SLC7 A5*-knockdown cell lines, MDA-MB-231 and HCC1937 cells were infected with *SLC7 A5* shRNA lentivirus. Infected cells were screened using 2 mg/L puromycin (BL528 A, Biosharp) for 48 h following the manufacturer's protocol to obtain stable cell lines.

Measurement of amino acids by LC–MS analysis

Quantitative analysis of amino acids and their derivatives in cell and tissue samples was conducted by Applied Protein Technology Co., Ltd. (Shanghai, China). Amino acid measurements were performed using liquid chromatography-tandem mass spectrometry (LC–MS/MS). Separation of cell and tissue samples was achieved using the Agilent 1290 Infinity ultra-high-performance liquid chromatography (UHPLC) system, while mass spectrometry analysis was conducted in positive ion mode with a 5500 QTRAP mass spectrometer (AB SCIEX). Chromatographic peak areas and retention times were extracted using Multiquant software. Standard compounds of amino acids and their derivatives were used to correct retention times for accurate metabolite identification.

Flow cytometry analysis

Flow cytometry (FACS) was used to analyze LAT1 and LAT2 expression on the cell surface. Cells were collected, washed, and resuspended in FACS buffer. Primary antibodies were added, and the samples were incubated at 4 °C in the dark for 30 min, followed by three washes and centrifugation. Secondary antibodies were then added, and the samples were incubated under the same conditions. Fluorescence signals were immediately detected using a flow cytometer (BD Biosciences). The antibodies used included PerCP-conjugated mouse monoclonal anti-LAT1 antibody (#NBP2-50465PCP, Novus Biologicals), unconjugated mouse monoclonal anti-LAT2 antibody (#MA5-24,943, Invitrogen), and Alexa Fluor 488 goat anti-mouse secondary antibody (#A28175, Invitrogen).

Proliferation assays

Cells (5×10^4 cells/well) were seeded into a 24-well plate. Once adhered, the cells were treated with fresh medium containing varying concentrations of JPH203 (Nanvuranlat, Selleck) or an equivalent volume of DMSO. Cultures were maintained for 48 h (MDA-MB-231, HCC1937, SK-BR-3, and T47D) or 96 h (BT474). Cell counts were normalized to DMSO controls, and dose-proliferation inhibition curves for JPH203 were plotted.

Cell cycle analysis

Cells (1×10^6 cells/well) were seeded into 6-well plates. Once adhered, the cells were treated with fresh medium containing varying concentrations of JPH203 or an equivalent volume of DMSO and cultured for 48 h. Cell samples were prepared following the Cell Cycle Assay Kit Plus (#C6078, UElandy Inc) protocol. Briefly, cells were collected, centrifuged, fixed in 70% cold ethanol, and stored overnight at − 20 °C. RedNucleus I staining solution was added, and the samples were incubated at room temperature in the dark for 20 min. Flow cytometry analysis was subsequently performed to assess cell cycle distribution.

Apoptosis assay

Cells (5×10^4 cells/well) were seeded into 6-well plates. Once adhered, the medium was replaced with fresh medium containing varying concentrations of JPH203 or an equivalent volume of DMSO, and cells were cultured for 48 h. Cells were collected and washed twice with phosphate buffer saline (PBS). Apoptosis was assessed using the Annexin

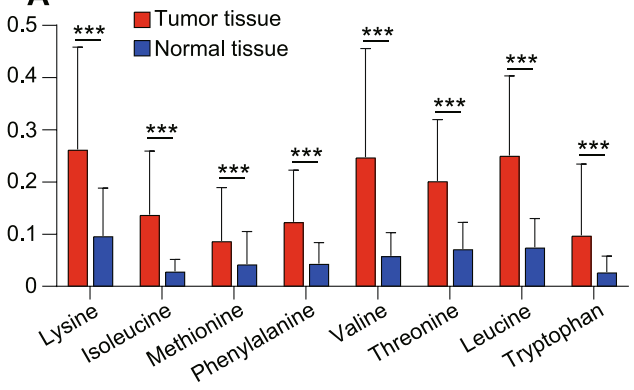
A
Tumor tissue
Normal tissue
0.5
0.4
0.3
0.2
0.1
0
***
Lysine
Isoleucine
Methionine
Phenylalanine
Valine
Threonine
Leucine
Tryptophan

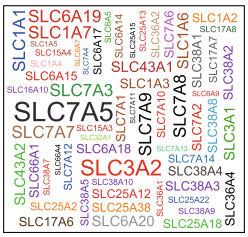
B
SLC1A1
SLC6A19
SLC1A7
SLC1A2
SLC17A8
SLC43A1
SLC6A15
SLC7A3
SLC1A3
SLC7A5
SLC7A7
SLC6A18
SLC7A9
SLC7A8
SLC3A2
SLC38A4
SLC43A2
SLC66A1
SLC7A14
SLC38A3
SLC25A12
SLC25A22
SLC25A2
SLC25A38
SLC38A9
SLC17A6
SLC6A20
SLC25A18
SLC36A4
SLC3A1

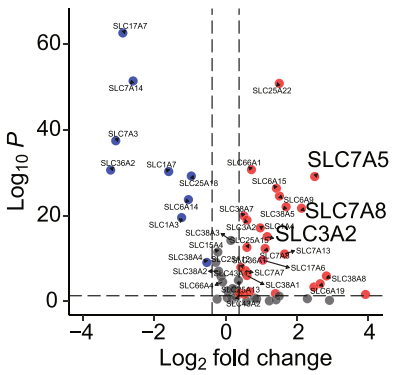
C
60
40
20
0
Log10 P
−4
−2
0
2
4
Log2 fold change
SLC7A5
SLC7A8
SLC3A2

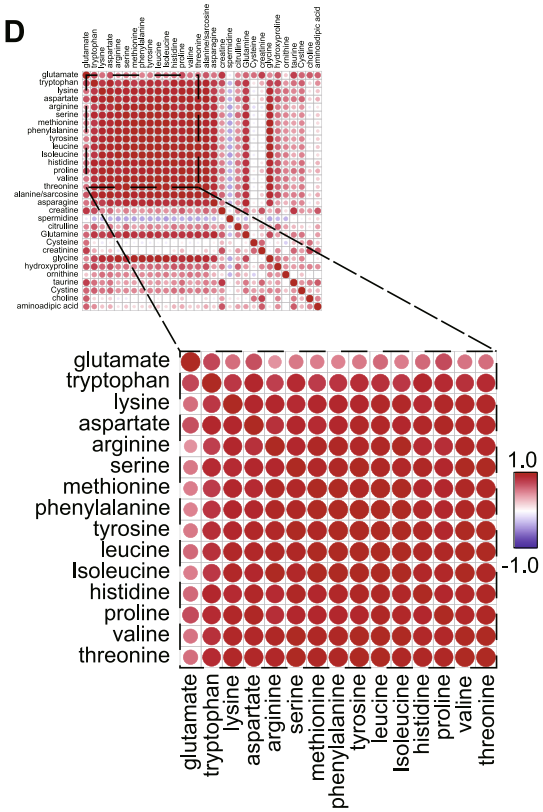
D
glutamate
tryptophan
lysine
aspartate
arginine
serine
methionine
phenylalanine
tyrosine
leucine
Isoleucine
histidine
proline
valine
threonine
1.0
-1.0

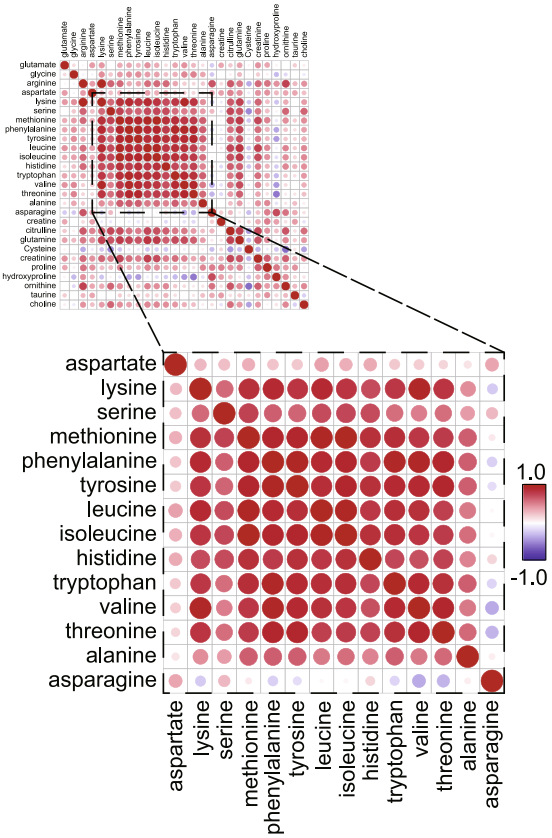
aspartate
lysine
serine
methionine
phenylalanine
tyrosine
leucine
isoleucine
histidine
tryptophan
valine
threonine
alanine
asparagine
1.0
-1.0

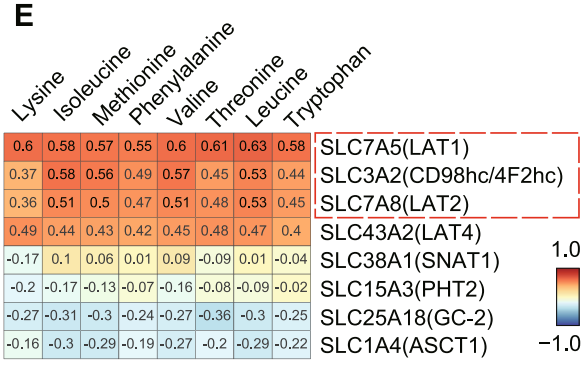
E
Lysine
Isoleucine
Methionine
Phenylalanine
Valine
Threonine
Leucine
Tryptophan
0.6 0.58 0.57 0.55 0.6 0.61 0.63 0.58 SLC7A5(LAT1)
0.37 0.58 0.56 0.49 0.57 0.45 0.53 0.44 SLC3A2(CD98hc/4F2hc)
0.36 0.51 0.5 0.47 0.51 0.48 0.53 0.45 SLC7A8(LAT2)
0.49 0.44 0.43 0.42 0.45 0.48 0.47 0.4 SLC43A2(LAT4)
-0.17 0.1 0.06 0.01 0.09 -0.09 0.01 -0.04 SLC38A1(SNAT1)
-0.2 -0.17 -0.13 -0.07 -0.16 -0.08 -0.09 -0.02 SLC15A3(PHT2)
-0.27 -0.31 -0.3 -0.24 -0.27 -0.36 -0.3 -0.25 SLC25A18(GC-2)
-0.16 -0.3 -0.29 -0.19 -0.27 -0.2 -0.29 -0.22 SLC1A4(ASCT1)
1.0
−1.0

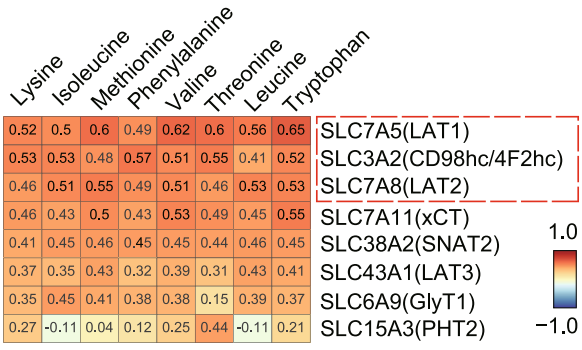
Lysine
Isoleucine
Methionine
Phenylalanine
Valine
Threonine
Leucine
Tryptophan
0.52 0.5 0.6 0.49 0.62 0.6 0.56 0.65 SLC7A5(LAT1)
0.53 0.53 0.48 0.57 0.51 0.55 0.41 0.52 SLC3A2(CD98hc/4F2hc)
0.46 0.51 0.55 0.49 0.51 0.46 0.53 0.53 SLC7A8(LAT2)
0.46 0.43 0.5 0.43 0.53 0.49 0.45 0.55 SLC7A11(xCT)
0.41 0.45 0.46 0.45 0.45 0.44 0.46 0.45 SLC38A2(SNAT2)
0.37 0.35 0.43 0.32 0.39 0.31 0.43 0.41 SLC43A1(LAT3)
0.35 0.45 0.41 0.38 0.38 0.15 0.39 0.37 SLC6A9(GlyT1)
0.27 -0.11 0.04 0.12 0.25 0.44 -0.11 0.21 SLC15A3(PHT2)
1.0
−1.0

◂**Fig. 1** Differential expression and correlation of EAAs and amino acid transporters in breast cancer. **A** Levels of essential amino acids (EAAs) in tumor tissue versus corresponding normal tissue samples from 36 breast cancer patients, analyzed using paired *t*-tests (***$p < 0.001$). **B** List of 60 known amino acid transporters. **C** Volcano plot illustrating the differences in transcript levels of 60 amino acid transporters between tumor and normal tissues (red: high expression in tumor, blue: low expression in tumor). **D** Correlation heatmap of 8 EAA levels in (left) 36 breast cancer tumor tissue samples and (right) 49 breast cancer cell lines. **E** Correlation heatmap between 8 EAAs and 23 highly expressed amino acid transporter transcript levels in (left) 36 tumor tissue samples and (right) 49 breast cancer cell lines. Correlation coefficients were determined using Pearson correlation analysis

V-FITC/7-AAD fluorescence dual staining kit (#P-CA-202, Procell Life Science Technology Co., Ltd) according to the manufacturer's protocol. Cells were resuspended in Annexin V Binding Buffer, and Annexin V-FITC and 7-AAD were added to the suspension. Samples were gently vortexed, incubated at room temperature in the dark for 15 min, and immediately analyzed using flow cytometry.

Cell counting kit-8 (CCK-8) assay

Cells (2,000 cells/well) were seeded into 96-well plates. After adherence, the medium was replaced with fresh medium containing the IC_{50} concentration of JPH203 or an equivalent volume of DMSO. Cells were cultured for 1–7 days, and cell viability was assessed using the CCK-8 kit (#B34304, Selleck). CCK-8 reagent (10 µL) was added to each well, and plates were incubated at 37 °C for 2 h. Absorbance was measured at 450 nm using a microplate reader.

Colony formation assay

Cells (300 cells/well) were seeded into 6-well plates. Once adhered, the medium was replaced with fresh medium containing the IC_{50} concentration of JPH203 or an equivalent volume of DMSO. Cells were cultured for 14 days, after which the medium was removed, and the cells were washed with PBS. Colonies were fixed with 4% paraformaldehyde at 4 °C for 10 min, stained with 2% crystal violet for 10 min, and washed with PBS. Plates were air-dried at room temperature, and colony formation was quantified.

Experimental animals

Twelve 7-week-old female BALB/c mice (SJA Laboratory Animal Co., Ltd, Hunan) were housed under specific pathogen-free (SPF) conditions. A suspension of 5×10^5 4 T1 cells in 0.1 mL culture medium was subcutaneously injected into the right axilla of each mouse. Once tumors formed, mice were randomly divided into two groups ($n = 6$/group). Body weight and tumor dimensions (length and width) were measured at baseline. Mice were intraperitoneally injected every other day with JPH203 (12.5 mg/kg) or an equivalent volume of DMSO. Tumor volume and body weight were recorded every two days. Following treatment, mice were euthanized, and tumor tissues were collected, photographed, and fixed in formalin for histological analysis. Blood samples were collected via the retro-orbital sinus for serum analysis of liver function using an automated biochemical analyzer (BS-420, Shenzhen Mindray).

Furthermore, Thirty-two 7-week-old female BALB/c mice were used to construct a 4 T1-BALB/c tumor-bearing model using the same protocol. After tumor formation, mice were randomly assigned to four groups ($n = 8$/group). On days 1, 4, 7, and 10 post-grouping, mice received intraperitoneal injections of anti-PD-1 antibody (100 µg; RMP1-14, Bio X Cell) or rat IgG, along with JPH203 (12.5 mg/kg) or DMSO. Tumor volume and weight were measured every two days. Tumor volume (mm^3) was calculated using the formula:

$$\text{Tumor volume}\,(mm^3) = length \times width^2/2$$

TUNEL assay

The TUNEL assay was performed using the In Situ Cell Death Detection Kit (11,684,817,910, Roche) following the manufacturer's instructions. Tissue sections were incubated with proteinase K solution (P1120, Solarbio) at room temperature for 15 min. Then, 50µL of TUNEL reaction mixture (enzyme: labeling solution = 1:9) was applied to each section and incubated at 37 °C in the dark for 60 min. After washing with PBS, 50µL of POD solution was added, followed by a 30-min incubation at 37 °C. Diaminobenzidine (DAB) staining (DA1010, Solarbio) was performed, and the sections were imaged under a microscope (DM1000, Leica). TUNEL-positive cells were quantified for analysis.

Immunohistochemistry (IHC)

Paraffin-embedded sections were deparaffinized, rehydrated, and subjected to antigen retrieval. The sections were blocked with 10% goat serum (SL038, Solarbio) to reduce nonspecific binding. Tumor sections from breast cancer patients were incubated overnight at 4 °C with primary antibodies targeting LAT1 (#PA5-115,916, Invitrogen) and LAT2 (#PA5-63,887, Invitrogen). After rewarming at

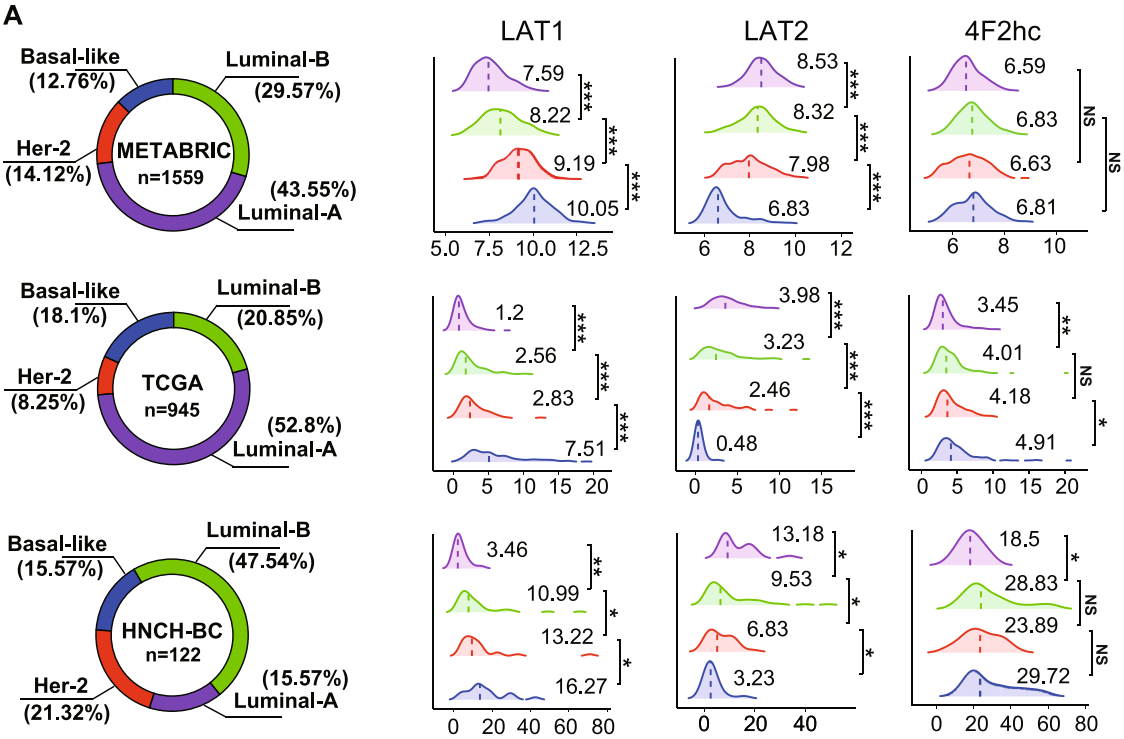
A
LAT1
LAT2
4F2hc
Basal-like (12.76%)
Luminal-B (29.57%)
Her-2 (14.12%)
METABRIC n=1559
(43.55%) Luminal-A
Basal-like (18.1%)
Luminal-B (20.85%)
Her-2 (8.25%)
TCGA n=945
(52.8%) Luminal-A
Basal-like (15.57%)
Luminal-B (47.54%)
HNCH-BC n=122
Her-2 (21.32%)
(15.57%) Luminal-A
7.59
8.22
9.19
10.05
8.53
8.32
7.98
6.83
6.59
6.83
6.63
6.81
1.2
2.56
2.83
7.51
3.98
3.23
2.46
0.48
3.45
4.01
4.18
4.91
3.46
10.99
13.22
16.27
13.18
9.53
6.83
3.23
18.5
28.83
23.89
29.72
NS

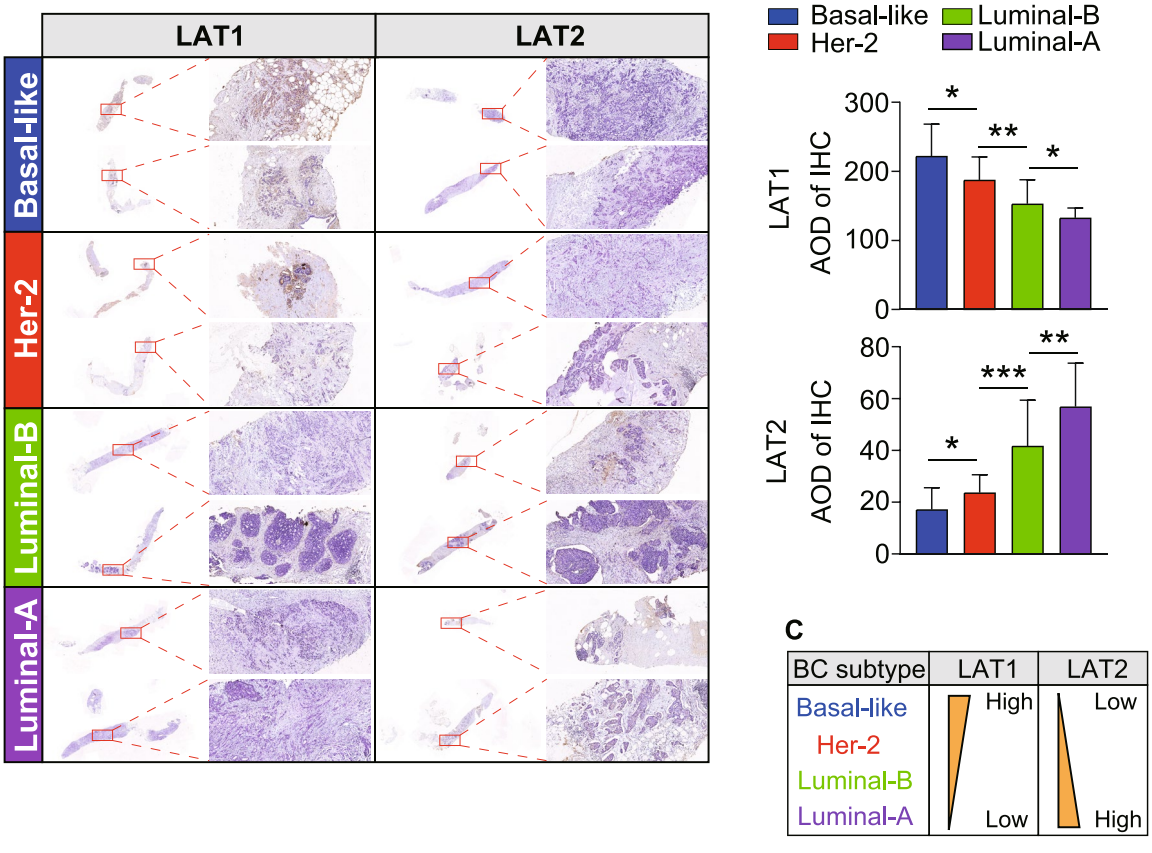
B
LAT1
LAT2
Basal-like
Her-2
Luminal-B
Luminal-A
Breast cancer subtype
Basal-like
Luminal-B
Her-2
Luminal-A
LAT1 AOD of IHC
LAT2 AOD of IHC
C
BC subtype
LAT1
LAT2
Basal-like
Her-2
Luminal-B
Luminal-A
High
Low
Low
High

◂**Fig. 2** Expression patterns of LAT1, LAT2, and 4F2 hc in breast cancer subtypes. **A** RNA-seq data from TCGA, METABRIC, and HNCH-BC databases showing the expression levels of LAT1 (*SLC7 A5*), LAT2 (*SLC7 A8*), and 4F2 hc (*SLC3 A2*) across different breast cancer subtypes. Donut charts indicate the distribution of molecular subtypes in each database, while mountain plots depict the differences in transcript levels (***$p < 0.001$). Immunohistochemistry (IHC) demonstrate LAT1 and LAT2 protein levels in tumor tissue samples. **B** Representative IHC images for LAT1 and LAT2 proteins in breast cancer subtypes ($n = 20$/subtype), quantified by average optical density (AOD) (*$p < 0.05$; **$p < 0.01$). **C** Distribution of LAT1 and LAT2 protein levels across breast cancer subtypes

room temperature for 30 min, sections were incubated with appropriate secondary antibodies. Similarly, mouse tumor tissue sections were incubated overnight with an anti-Ki67 primary antibody (#1222 T, CST) at 4 °C and treated with a MaxVision HRP polymer anti-mouse/rabbit secondary antibody (KIT-5020, Maixin Biotechnology Co., Ltd.) for 60 min at room temperature. Samples were stained with DAB (DA1010, Solarbio), counterstained with hematoxylin (G1004, Servicebio) for 3 min, and analyzed under a microscope (DM1000, Leica).

Multiplex immunohistochemistry (m-IHC)

Multiplex IHC was performed by Aikefa Biotechnology Co., Ltd. (Beijing, China). The staining procedure was conducted using an Alphapeiner instrument. Primary antibodies targeting CD8, CD4, FOXP3, and PD-L1, along with corresponding secondary antibodies, were applied sequentially. Fluorescent labeling of secondary antibodies was followed by DAPI nuclear counterstaining after four cycles of labeling. Stained sections were sealed with an anti-fade mounting medium and analyzed using a fluorescence scanning imaging system. Protein expression levels for CD8, CD4, FOXP3, and PD-L1 were quantified using HALO analysis software (version 3.5, Indica Labs, United States).

Statistical analysis

Statistical analyses were conducted using GraphPad Prism V.7.0 software. Paired *t*-tests were performed for matched data, while Pearson correlation analysis was used to evaluate correlations between variables. RNA-seq data from the TCGA, METABRIC, and HNCH-BC databases were analyzed using the Wilcoxon test. Experimental data were analyzed using unpaired Student's *t*-tests. Data are presented as mean ± standard deviation (SD). Statistical significance was defined as $p < 0.05$, with Not significant (ns): $p > 0.05$; *$p < 0.05$; **$p < 0.01$; ***$p < 0.001$.

Results

LAT1, LAT2, and 4F2 hc as key transporters for the EAAs uptake in breast cancer

Comparative analysis of RNA-seq and metabolomics data from tumor and normal tissues of 36 breast cancer patients revealed significantly elevated concentrations of eight EAAs in tumor tissues (Fig. 1A). Moreover, 32 of 60 amino acid transporter transcripts showed increased expression in breast cancer tissues (Fig. 1C). Correlation analysis of 20 amino acid levels demonstrated a strong association between the levels of the eight EAAs in both breast cancer tissues and cell lines (Fig. 1D). Further investigation into the association between EAA levels and transporter expression showed a strong correlation between LAT1 (*SLC7 A5*), LAT2 (*SLC7 A8*), and 4F2 hc (*SLC3 A2*) transcript levels and EAA concentrations (Fig. 1E). These findings highlight the important role of LAT1, LAT2, and 4F2 hc in the uptake of EAAs in breast cancer.

High reliance of TNBC on LAT1 for EAA uptake

Analysis of RNA-seq data from the TCGA, METABRIC, and HNCH-BC databases was conducted to evaluate the distribution of the aforementioned transporters across breast cancer subtypes. Transcriptional levels of LAT1, LAT2 and 4F2 hc varied among different breast cancer subtypes. Consistent across all databases, LAT1 showed the highest transcriptional levels in TNBC, followed by Her-2-positive, and the lowest in luminal subtypes. LAT2 displayed an inverse trend, while 4F2 hc levels showed no significant differences among these subtypes (Fig. 2A). Immunohistochemical analysis of tumor tissues from various breast cancer subtypes confirmed the subtype-specific distribution. LAT1 expression was highest in TNBC tissues, followed by Her-2-positive, and lowest in luminal subtypes. On the contrary, LAT2 expression was highest in luminal subtypes and lowest in TNBC (Fig. 2B and C).

Breast cancer cell lines representing different molecular subtypes were analyzed to further validate these observations. LAT1 and LAT2 transcript levels were quantified using qRT-PCR (Fig. 3A), surface protein levels were assessed via flow cytometry (Fig. 3B). Results consistently confirmed that TNBC cell lines had the highest LAT1 expression and the lowest LAT2 expression compared to other subtypes. These findings demonstrate that TNBC cells primarily rely on LAT1 for EAA uptake, providing

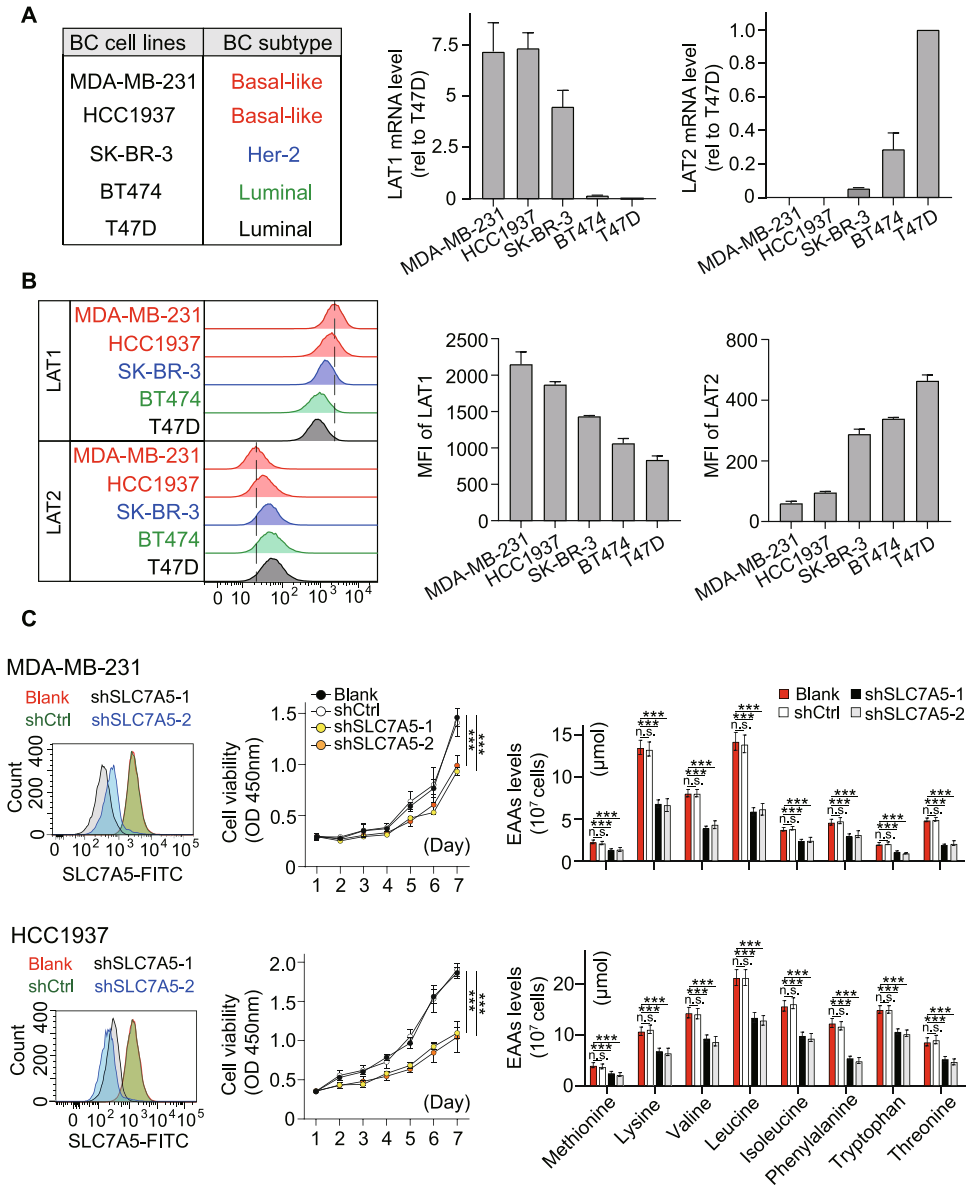

Fig. 3 Therapeutic potential of targeting LAT1 in TNBC. **A** Quantitative analysis of *LAT1* and *LAT2* transcript levels in five breast cancer cell lines (MDA-MB-231, HCC1937, SK-BR-3, BT474, and T47D) using qRT-PCR, normalized to GAPDH and plotted as fold changes relative to T47D. **B** Flow cytometry analysis showing LAT1 and LAT2 protein expression on the cell surface of breast cancer cell lines, expressed as mean fluorescence intensity (MFI). **C** LAT1 knockdown using shRNA (shSLC7 A5-1 or shSLC7 A5-2) in MDA-MB-231 and HCC1937 cells. Flow cytometry validated LAT1 expression levels (Bank: wild type; shCtrl: empty shRNA). Proliferation was assessed using the CCK-8 assay (***$p < 0.001$), and EAA levels were analyzed via metabolomics (***$p < 0.001$). Data are presented as mean ± SD from three independent experiments

a molecular rationale for targeting LAT1 to inhibit EAA transport and disrupt TNBC metabolism.

Targeting of LAT1 can limit EAA uptake and inhibit the TNBC cell proliferation in vitro

To investigate LAT1's role in TNBC cell proliferation, *SLC7 A5*-specific shRNA was delivered via lentiviral vectors to downregulate LAT1 expression in MDA-MB-231 and HCC1937 cells (Fig. 3C). Proliferation assays and metabolomics analyses revealed significant reductions in TNBC cell proliferation and EAA uptake following LAT1 knockdown (Fig. 3C). To increase the clinical translational value, cells were treated with varying concentrations of the LAT1-specific inhibitor JPH203. Dose–response curves demonstrated that JPH203 inhibited the proliferation of all breast cancer subtypes in a dose-dependent manner. TNBC cell lines (MDA-MB-231 and HCC1937) showed significantly lower IC_{50} values compared to Her-2 and luminal subtypes,

indicating greater sensitivity due to a stronger reliance on LAT1 for EAA uptake (Fig. 4A).

Cell cycle and apoptosis assays further elucidated the mechanism of action. JPH203 treatment resulted in a dose-dependent increase in G2/M phase arrest and apoptotic cells after 48 h in MDA-MB-231 and HCC1937 cells (Fig. 4B and C). Experimental validation using human TNBC cell lines (MDA-MB-231, HCC1937) and mouse TNBC cells (4 T1) confirmed that JPH203 significantly inhibited TNBC cell proliferation at IC_{50} concentrations (MDA-MB-231: 2.53 μM, HCC1937: 7.86 μM, 4 T1: 3.34 μM) in a time-dependent manner (Fig. 5A and Supplementary Fig. 1 A). Clone forming assays revealed a significant reduction in colony formation (Fig. 5B). Furthermore, metabolomics analysis showed a significant decrease in EAA levels in TNBC cells following JPH203 treatment (Fig. 5C). These findings highlight JPH203's efficacy in inhibiting TNBC cell proliferation and EAA uptake in vitro.

JPH203 demonstrates anti-tumor effects and reshapes the tumor immune microenvironment in vivo

Based on the highest sensitivity of TNBC cells to JPH203 observed in vitro, 4 T1 cells were used to establish a subcutaneous tumor model in BALB/c mice with intact immune systems (Fig. 6A). Intraperitoneal administration of JPH203 (12.5 mg/kg) significantly inhibited tumor growth compared to vehicle (DMSO) controls (Fig. 6B). Comprehensive metabolomics, IHC, and m-IHC analyses were performed to evaluate tumor EAA levels, proliferation markers (Ki67), apoptosis markers (TUNEL), and changes in immune cell populations within the tumor microenvironment. JPH203 treatment led to reduced EAA levels (Fig. 6C) and Ki67 expression, alongside an increase in TUNEL-positive apoptotic cells (Fig. 6D) within tumor tissues. Furthermore, immunological assessments revealed an increase in $CD8^+$ T cells and a decrease in regulatory T cells (Tregs) and PD-L1-positive cells in the tumor microenvironment (Fig. 6E). Importantly, JPH203 treatment did not induce hepatotoxicity or cause significant weight fluctuations in mice, demonstrating its safety profile (Fig. 6B and Supplementary Fig. 1B). These in vivo findings establish that JPH203 restricts EAA uptake, suppresses tumor proliferation, induces apoptosis, and remodels the suppressive immune microenvironment in TNBC without adverse effects.

To explore the potential synergy between JPH203 and immune checkpoint inhibitors, tumor-bearing 4 T1-BALB/c mice (n = 8/group) were treated with JPH203, PD-1 antibody, or a combination of both (Fig. 6F). Combination therapy significantly enhanced tumor growth inhibition and reduced tumor weight compared to monotherapy or control treatments (Fig. 6G and Supplementary Fig. 1 C). No significant differences in body weight were observed across the groups. These results suggest that JPH203 improves the therapeutic efficacy of PD-1 antibodies by reshaping the immune microenvironment, exerting synergistic anti-tumor effects.

Discussion

Despite recent advances in TNBC treatment, including the development of immunotherapy, drug resistance remains a critical challenge in clinical practice. With the growing focus on tumor metabolism in cancer research, targeting metabolic pathways offers a promising therapeutic approach (Faubert et al. 2020). Preclinical studies have demonstrated that EAA metabolism not only influences the biological behavior of breast cancer cells but also contributes to therapeutic resistance and the formation of an immunosuppressive tumor microenvironment (Lu et al. 2021; Saito et al. 2019; Chen et al. 2014). Therefore, identifying and targeting EAA metabolism may represent a novel strategy for TNBC therapy. In line with this concept, the present study used JPH203 to target LAT1, thereby blocking the uptake of exogenous EAAs. This approach successfully induced amino acid starvation, cell cycle arrest, and apoptosis in TNBC cells. Moreover, the study confirmed the anti-tumor activity and safety of JPH203 in vivo, particularly its ability to reshape the tumor immune microenvironment. These findings highlight the potential therapeutic value of targeting LAT1 in TNBC and provide a foundation for further exploration of this approach in TNBC immunotherapy.

Metabolic reprogramming is a hallmark of cancer (Kim and DeBerardinis 2019). Under normal conditions, glucose serves as the primary energy and carbon source for cells. However, tumor cells show a phenomenon known as the"Warburg effect,"where approximately 80% of glucose is converted to lactate via glycolysis and excreted, with only a small fraction of pyruvate entering the tricarboxylic acid (TCA) cycle (Koppenol et al. 2011). Therefore, tumor cells rely heavily on alternative carbon sources to sustain TCA cycle activity. Amino acids are among the primary carbon sources supporting tumor cell proliferation (Hosios et al. 2016). Eight of the 20 amino acids essential for protein synthesis in humans are classified as EAAs because neither normal nor cancer cells can synthesize

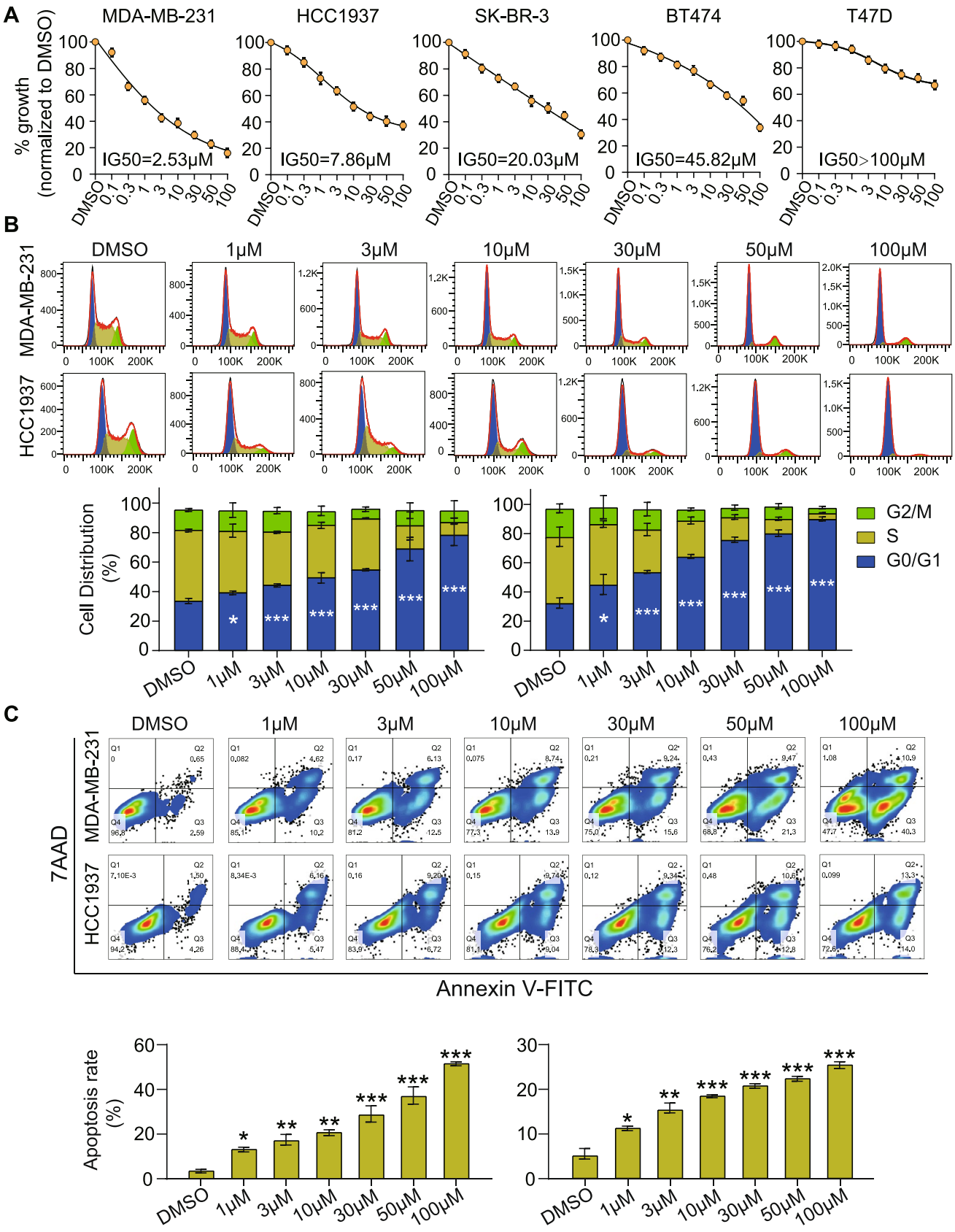
A
MDA-MB-231
HCC1937
SK-BR-3
BT474
T47D
% growth (normalized to DMSO)
IG50=2.53μM
IG50=7.86μM
IG50=20.03μM
IG50=45.82μM
IG50>100μM
DMSO
0.1
0.3
1
3
10
30
50
100
B
DMSO
1μM
3μM
10μM
30μM
50μM
100μM
MDA-MB-231
HCC1937
Cell Distribution (%)
G2/M
S
G0/G1
C
7AAD
Annexin V-FITC
Apoptosis rate (%)

◂**Fig. 4** Effects of JPH203 on breast cancer cell proliferation, cell cycle, and apoptosis. **A** Dose–response curves for breast cancer cell lines (MDA-MB-231, HCC1937, SK-BR-3, BT474, and T47D) treated with varying concentrations of JPH203 (0.1–100 μM) or DMSO. Cells were incubated for 48 h (96 h for BT474). Proliferation was normalized to the DMSO control, and IC_{50} values were calculated. **B** The cell cycle distribution of MDA-MB-231 and HCC1937 cells treated with JPH203 or DMSO, analyzed by flow cytometry. Bar charts show the mean cell percentages ± SD in each cycle stage across three independent experiments (*$p < 0.05$; ***$p < 0.001$). **C** Apoptosis rates of MDA-MB-231 and HCC1937 cells treated with JPH203 or DMSO, analyzed by flow cytometry. Bar charts display the mean cell percentages ± SD for each experimental group across three independent experiments (*$p < 0.05$; **$p < 0.01$; ***$p < 0.001$)

them. Instead, they rely on amino acid transporters for transmembrane transport. Thus, targeting amino acid transporters to limit EAA uptake is a feasible strategy for breast cancer therapy. Among the 60 known amino acid transporters, LAT1 and LAT2 are the principal mediators of EAA uptake. These transporters form functional complexes with the 4 F2 hc heavy chain to execute amino acid transport. Consistent with previous reports, this study observed strong correlations between the levels of eight EAAs in breast cancer tissues and cell lines and the levels of LAT1, LAT2, and 4 F2 hc transporters, indicating their critical roles in EAA transport in breast cancer. Although LAT1 and LAT2 share similar structures and amino acid substrates, their expression patterns show obvious tumor and tissue specificity. The study revealed significant and consistent differences in LAT1 and LAT2 expression levels across different molecular subtypes of breast cancer. LAT1 was most highly expressed in TNBC, followed by the Her-2 subtype, with the lowest levels in the Luminal subtype. However, LAT2 showed an inverse pattern. Given the predominance of LAT1 and lack of LAT2 in TNBC, LAT1 serves as the primary transporter facilitating EAA uptake in TNBC cells. These findings highlight LAT1 as a critical molecular target for disrupting EAA metabolism in TNBC, providing the foundation for more effective therapeutic strategies.

The level of LAT1 expression is notably higher in tumor cells compared to normal tissues, which is associated with the increased metabolic demands of cancer cells. This differential expression not only highlights LAT1's role in cancer metabolism but also positions it as a potential biomarker for tumor aggressiveness and a target for therapeutic strategies. Elena et al. (Ansari et al. 2018), found that LAT1 expression in TNBC was higher than in other breast cancer subtypes, which aligns with our findings. In addition, recent studies (Ichinoe et al. 2021 Sep; Furuya et al. 2012 Feb) have highlighted the significant role of LAT1 in TNBC prognosis, where elevated LAT1 levels correlate with increased cell proliferation, lymph-node metastasis and poorer patient survival. As such, LAT1 has emerged as a promising biomarker for predicting prognosis and a potential therapeutic target in TNBC treatment strategies.

Previous studies have demonstrated that LAT1 downregulation inhibits cell proliferation in prostate and gastric cancers in vitro, but it does not affect ovarian cancer cell proliferation, suggesting a tissue-specific effect (Wang et al. 2013; Shi et al. 2013; Fan et al. 2010). To evaluate the therapeutic potential of targeting LAT1 in TNBC, this study first employed shRNA-mediated *SLC7 A5* gene knockout, which significantly reduced TNBC cell proliferation and EAA levels. To increase the clinical translational value, the LAT1-specific inhibitor JPH203 was then used for experimental validation. JPH203, a highly selective LAT1 inhibitor, is currently the only effective compound of its kind (Okunushi et al. 2020). Several in vitro studies have confirmed its ability to inhibit the proliferation of medulloblastoma, osteosarcoma, and oral cancer cells (Cormerais et al. 2019; Yun et al. 2014; Choi et al. 2017). In 2020, the first phase I clinical trial of JPH203 in Japan, conducted on patients with advanced solid tumors (primarily cholangiocarcinoma), demonstrated its favorable biosafety (Okano et al. 2020). Besides, inhibiting the LAT1/CD98 pathway with JPH203 during the precancerous stage could suppress tumorigenesis in mutp53-driven thymic lymphoma models (Yao et al. 2023). Therefore, JPH203 is considered a safe and promising anti-cancer agent with significant clinical potential. However, research on JPH203 in breast cancer, particularly TNBC, remains limited, with no prior reports of its effects on TNBC cell growth in vivo or in vitro. This study addresses this gap by investigating the therapeutic efficacy and mechanisms of JPH203 in TNBC.

Our in vitro experiments revealed that JPH203 induced EAA starvation and G0/G1 phase cell cycle arrest in breast cancer cells, leading to inhibition of proliferation and apoptosis. Interestingly, sensitivity to JPH203 varied across breast cancer subtypes, following the order TNBC > Her-2 > Luminal. This disparity likely reflects differences in LAT1 and LAT2 transporter expression levels on the surface of different subtypes of breast cancer cells. TNBC cells, characterized by high LAT1 and low LAT2 expression, show the greatest dependence on LAT1 for EAA uptake, making them particularly sensitive to JPH203. These findings highlight the importance of considering tumor metabolic heterogeneity and vulnerability when developing targeted therapies. Stratification based on EAA metabolic dependency

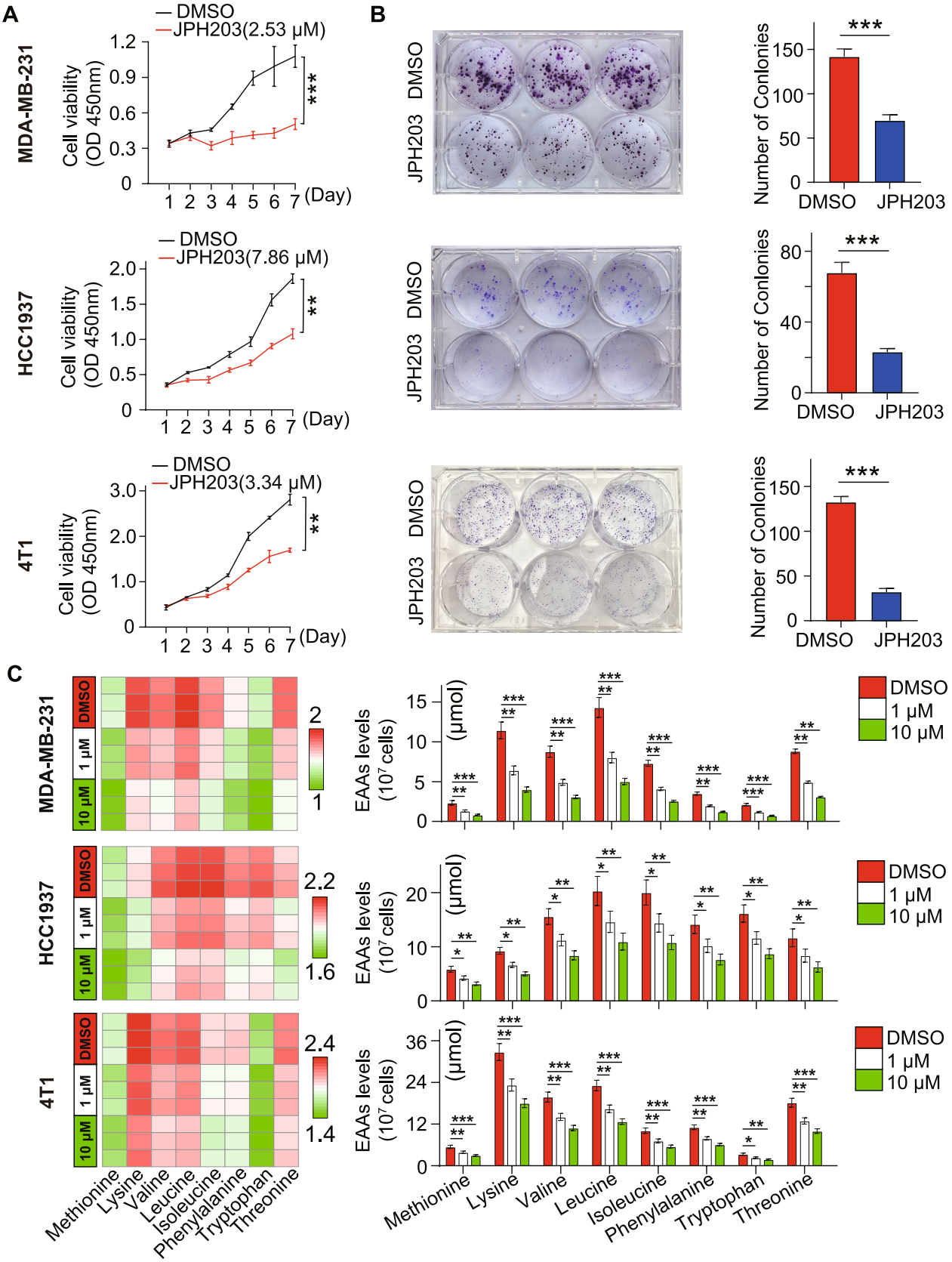
A
MDA-MB-231
DMSO
JPH203(2.53 μM)
Cell viability (OD 450nm)
(Day)
***
HCC1937
DMSO
JPH203(7.86 μM)
Cell viability (OD 450nm)
(Day)
**
4T1
DMSO
JPH203(3.34 μM)
Cell viability (OD 450nm)
(Day)
**
B
DMSO
JPH203
Number of Conlonies
DMSO
JPH203
***
C
MDA-MB-231
HCC1937
4T1
DMSO
1 μM
10 μM
EAAs levels (10^7 cells) (μmol)
Methionine
Lysine
Valine
Leucine
Isoleucine
Phenylalanine
Tryptophan
Threonine

◂**Fig. 5** Effects of JPH203 on TNBC cell proliferation, colony formation, and EAAs metabolism. **A** Proliferation curves of MDA-MB-231, HCC1937, and 4T1 cells treated with DMSO or IC_{50} concentrations of JPH203 (MDA-MB-231: 2.53 μM, HCC1937: 7.86 μM, 4T1: 3.34 μM) for 1–7 days, assessed using the CCK-8 method (**$p < 0.01$; ***$p < 0.001$). **B** Clone formation assay for MDA-MB-231, HCC1937, and 4T1 cells treated with DMSO or IC_{50} concentrations of JPH203 for 14 days. Representative images of the assay and bar charts of the mean ± SD from three experiments are shown (***$p < 0.001$). **C** Metabolomics analysis of EAAs levels in MDA-MB-231, HCC1937, and 4T1 cells treated with DMSO or JPH203 (1 μM and 10 μM) for 24 h. Bar charts present the mean ± SD from three independent experiments (*$p < 0.05$; **$p < 0.01$; ***$p < 0.001$)

may optimize the therapeutic efficacy of LAT1-targeted treatments. To further evaluate the anti-tumor activity of JPH203 in vivo, a 4 T1-BALB/c mouse subcutaneous tumor model was established and treated with the inhibitor JPH203. JPH203 treatment reduced intratumoral EAA concentrations slowed tumor growth, decreased Ki67 expression, and significantly increased apoptotic cell proportions. Importantly, JPH203 did not induce weight changes or liver toxicity in treated mice, further supporting its safety profile. These results collectively indicate that LAT1 inhibition with JPH203 effectively suppresses TNBC progression through metabolic disruption, presenting a potential therapeutic strategy for TNBC.

In the tumor microenvironment, both tumor and immune cells depend on EAAs to maintain normal metabolism and function. A deficiency in EAAs within this environment promotes the development of an immunosuppressive microenvironment, facilitating tumor progression and resistance to immunotherapy (Leone and Powell 2020). Key components of this immunosuppressive environment include PD-L1 expression and Tregs infiltration. Our previous findings revealed that TNBC patients with high intratumoral EAA levels show significantly elevated PD-L1 expression and increased Tregs infiltration compared to those with low EAA levels (Zhao et al. 2022). This clinical observation suggests that the competitive uptake of EAAs by TNBC cells may contribute to the establishment of an immunosuppressive microenvironment. Emerging evidence indicates that methionine competition by tumor cells in the microenvironment inhibits T cell immune function and induces T cell apoptosis (Bian et al. 2020). Moreover, a reduction in leucine and an accumulation of tryptophan metabolites can lead to an increase in Tregs proportions (Makowski et al. 2020). Based on JPH203's ability to inhibit EAAs uptake by TNBC cells, these findings provide a mechanistic basis for the hypothesis that JPH203 may reduce PD-L1 expression and Tregs infiltration in the TNBC microenvironment. In this study, analysis of tumor tissues from JPH203-treated mice revealed a significant increase in $CD8^+$ T cells, along with reduced PD-L1 expression and Tregs infiltration. Furthermore, the combination of JPH203 and PD-1 inhibitors resulted in enhanced anti-tumor effects, as demonstrated in animal models. These findings suggest that JPH203 mediates non-cell-autonomous tumor suppression by reshaping the tumor microenvironment and improving immune responsiveness. Overall, this study raises some exciting questions regarding the synergistic effects of JPH203 and PD-1 inhibitors, emphasizing the potential of their combination as a strategy to improve the efficacy of TNBC immunotherapy.

This study has multiple limitations and an exploratory nature. First, based on the levels of LAT1 expression in different subtypes of breast cancer and the results of the JPH203 dose-proliferation curve, we propose that luminal breast cancer is less sensitive to JPH203 treatment compared to other subtypes. However, this does not imply that luminal breast cancer cannot benefit from EAAs deprivation therapy. (Saito et al. 2019) found that leucine not only promotes the proliferation of luminal breast cancer cells but also contributes to the resistance of luminal breast cancer to tamoxifen. Moreover, this study only validated two luminal breast cancer cell lines (BT474 and T47D), indicating that more in vivo and in vitro experimental data are needed to further support this hypothesis. Furthermore, we did not investigate the metabolic adaptive changes in TNBC cells in response to LAT1 inhibition. In fact, inhibition of LAT1 allows cancer cells to upregulate other amino acid transporters or metabolic pathways to increase EAAs uptake, which can lead to the emergence of acquired resistance. Despite these limitations, our findings offer new insights that could inform future research on TNBC treatment.

Conclusion

This study is the first to delineate the distribution and functional significance of EAA transporters across different molecular subtypes of breast cancer, establishing the therapeutic value of targeting LAT1 for TNBC. By inhibiting LAT1 with JPH203, exogenous EAA uptake is blocked, leading to amino acid starvation, cell cycle arrest, and apoptosis in TNBC cells. Moreover, this study provides the first evidence of the anti-tumor activity and safety of JPH203 in vivo using a TNBC tumor-bearing mouse model with normal immune function. Importantly, JPH203 reshaped the immunosuppressive tumor microenvironment by reducing PD-L1 expression and Tregs infiltration, thereby enhancing the efficacy of PD-1 antibody therapy. These findings

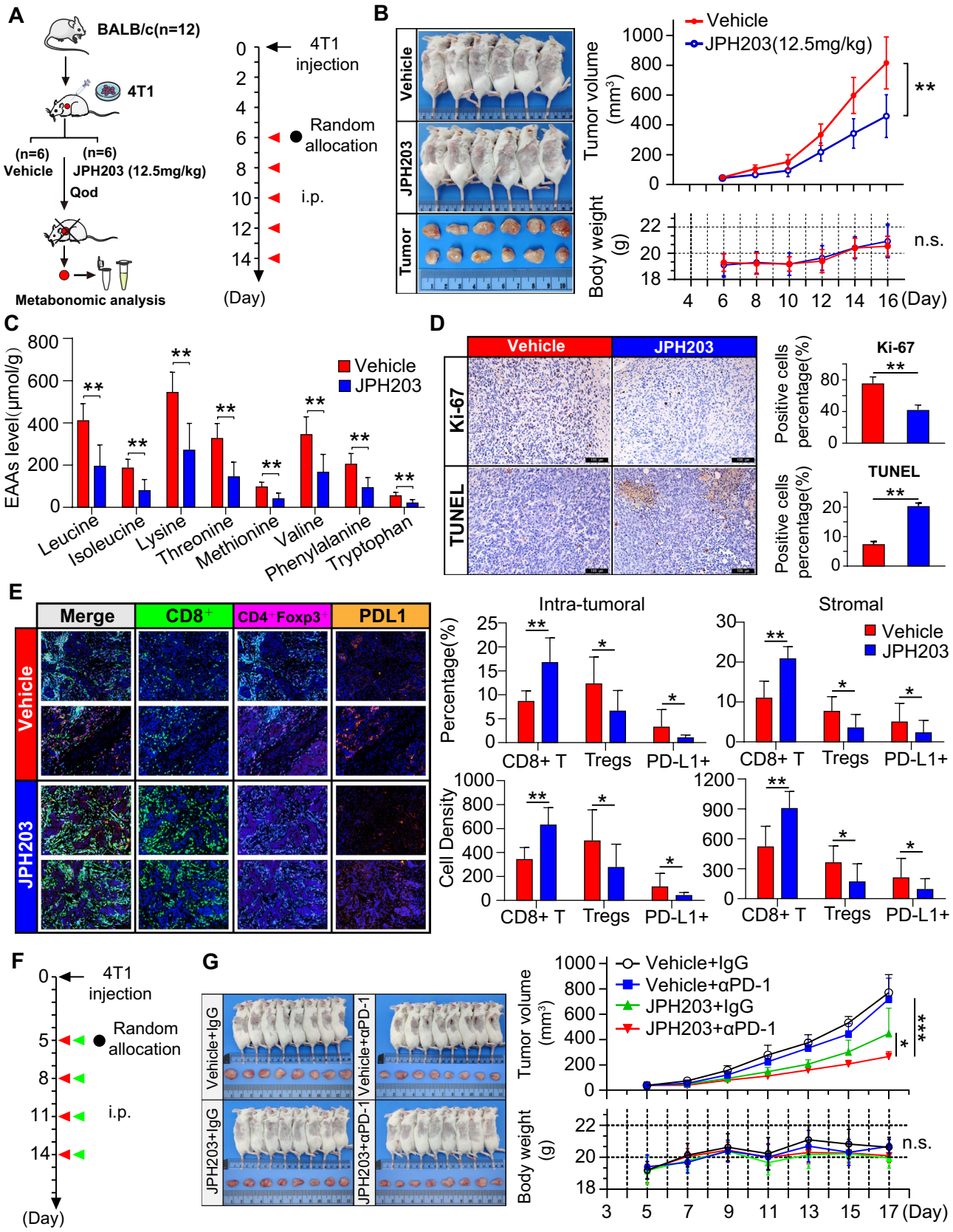
A
BALB/c(n=12)
4T1
(n=6) Vehicle
(n=6) JPH203 (12.5mg/kg)
Qod
Metabonomic analysis
4T1 injection
Random allocation
i.p.
(Day)
B
Vehicle
JPH203
Tumor
Tumor volume (mm3)
Vehicle
JPH203(12.5mg/kg)
Body weight (g)
n.s.
C
EAAs level(μmol/g)
Vehicle
JPH203
Leucine
Isoleucine
Lysine
Threonine
Methionine
Valine
Phenylalanine
Tryptophan
D
Vehicle
JPH203
Ki-67
TUNEL
Positive cells percentage(%)
E
Merge
CD8+
CD4+Foxp3+
PDL1
Intra-tumoral
Stromal
Percentage(%)
Cell Density
CD8+ T
Tregs
PD-L1+
F
4T1 injection
Random allocation
i.p.
(Day)
G
Vehicle+IgG
Vehicle+αPD-1
JPH203+IgG
JPH203+αPD-1
Tumor volume (mm3)
Body weight (g)
n.s.

◂**Fig. 6** Effects of JPH203 and combined treatments on 4T1-BALB/c tumor-bearing mice. **A** Treatment plan summary, with 6 mice per group. Tumor volume and body weight were recorded every 2 days, and tumors were removed at the endpoint of the experiment. **B** Representative images of tumors. Tumor growth curves and body weight changes. Data are represented as mean ± SD (**$p < 0.01$). **C** Metabolomics analysis of EAAs levels in 4T1 tumor tissues. Bar charts display the differences between treatment groups, presented as mean ± SD (n = 6/group) (**$p < 0.01$). **D** IHC detection of Ki67 and Tunel expression in tumor tissues (× 200). Bar charts show the proportion of Ki67 and Tunel-positive cells, presented as mean ± SD (n = 6/group) (**$p < 0.01$). **E** Multiplex IHC analysis of PD-L1(+) cells, $CD8^+$ T cells, and Tregs ($CD4^+Foxp3^+$) in the tumor parenchyma and stroma. Bar charts illustrate the density and percentage of these cell subsets, expressed as mean ± SD (n = 6/group) (*$p < 0.05$; **$p < 0.01$). **F** Treatment plan summary for 4T1-BALB/c tumor-bearing mice treated with JPH203 and/or PD-1 antibodies, with 8 mice per group. **G** Representative tumor images. Tumor growth curves and mouse weight changes. Data are presented as mean ± SD (n = 8/group) (*$p < 0.05$; ***$p < 0.001$)

highlight the potential of targeting EAA metabolism as a novel approach to improve TNBC immunotherapy. Furthermore, JPH203 emerges as a promising candidate for combination therapy with PD-1 inhibitors, offering a new therapeutic approach for TNBC treatment.

Supplementary Information The online version contains supplementary material available at https://doi.org/10.1007/s00726-025-03456-3.

Acknowledgements The results shown here are part based upon data generated by the TCGA Research Network: https://www.cancer.gov/tcga.

Author contributions Yajie Zhao conducted experiments. Zhenzhen Liu and Kangdong Liu designed experiments. Yajie Zhao and Chunrui Pu contributed to data analysis and prepared the manuscript. All authors supervised and approved the submitted version.

Funding This work was supported by the natural science foundation of henan province (242300420418) and Henan Provincial Science and Technology Research Project (252102311079).

Data availability The RNA-seq and metabolomic data in 49 breast cancer cell lines were downloaded from CCLE public database (https://portals.broadinstitute.org/ccle). Transcriptional levels of LAT1, LAT2 and 4F2 hc were analyzed from TCGA and METABRIC, downloaded from cBioPortal (https://www.cbioportal.org/).

Declarations

Conflict of interest The authors declare no competing interests.

Ethics approval Biological specimen collection of patients was approved by the Ethics Committee of Zhengzhou University Cancer Hospital (Zhengzhou, China; approval number HNCH-BC006), and written informed consent was obtained from all patients. The Ethics Review Committee for Life Sciences at Zhengzhou University has evaluated the animal experiment, confirming that both the research content and methodology of this project adhere to the ethical standards set forth by international and national guidelines for the welfare of experimental animals.

Open Access This article is licensed under a Creative Commons Attribution-NonCommercial-NoDerivatives 4.0 International License, which permits any non-commercial use, sharing, distribution and reproduction in any medium or format, as long as you give appropriate credit to the original author(s) and the source, provide a link to the Creative Commons licence, and indicate if you modified the licensed material. You do not have permission under this licence to share adapted material derived from this article or parts of it. The images or other third party material in this article are included in the article's Creative Commons licence, unless indicated otherwise in a credit line to the material. If material is not included in the article's Creative Commons licence and your intended use is not permitted by statutory regulation or exceeds the permitted use, you will need to obtain permission directly from the copyright holder. To view a copy of this licence, visit http://creativecommons.org/licenses/by-nc-nd/4.0/.

References

Adams S, Loi S, Toppmeyer D et al (2019) Pembrolizumab monotherapy for previously untreated, PD-L1-positive, metastatic triple-negative breast cancer: cohort B of the phase II KEYNOTE-086 study. Ann Oncol 30(3):405–411

Bian Y, Li W, Kremer DM et al (2020) Cancer SLC43A2 alters T cell methionine metabolism and histone methylation. Nature 585(7824):277–282

Chen JY, Li CF, Kuo CC et al (2014) Cancer/stroma interplay via cyclooxygenase-2 and indoleamine 2,3-dioxygenase promotes breast cancer progression. Breast Cancer Res 16(4):410

Choi DW, Kim DK, Kanai Y et al (2017) JPH203, a selective L-type amino acid transporter 1 inhibitor, induces mitochondria-dependent apoptosis in Saos2 human osteosarcoma cells. Korean J Physiol Pharmacol 21(6):599–607

Cormerais Y, Pagnuzzi-Boncompagni M, Schrötter S et al (2019) Inhibition of the amino-acid transporter LAT1 demonstrates anti-neoplastic activity in medulloblastoma. J Cell Mol Med 23(4):2711–2718

Cortes J, Cescon DW, Rugo HS et al (2020) Pembrolizumab plus chemotherapy versus placebo plus chemotherapy for previously untreated locally recurrent inoperable or metastatic triple-negative breast cancer (KEYNOTE-355): a randomised, placebo-controlled, double-blind, phase 3 clinical trial. Lancet 396(10265):1817–1828

Dey P, Kimmelman AC, DePinho RA (2021) Metabolic codependencies in the tumor microenvironment. Cancer Discov 11(5):1067–1081

El Ansari R, Craze ML, Miligy I et al (2018) The amino acid transporter SLC7A5 confers a poor prognosis in the highly proliferative breast cancer subtypes and is a key therapeutic target in luminal B tumours. Breast Cancer Res 20(1):21

Fan X, Ross DD, Arakawa H et al (2010) Impact of system L amino acid transporter 1 (LAT1) on proliferation of human ovarian cancer cells: a possible target for combination therapy with antiproliferative aminopeptidase inhibitors. Biochem Pharmacol 80(6):811–818

Faubert B, Solmonson A, DeBerardinis RJ (2020) Metabolic reprogramming and cancer progression. Science 368(6487):5473

Feng M, Xiong G, Cao Z et al (2018) LAT2 regulates glutamine-dependent mTOR activation to promote glycolysis and chemoresistance in pancreatic cancer. J Exp Clin Cancer Res 37(1):274

Furuya M, Horiguchi J, Nakajima H et al (2012) Correlation of L-type amino acid transporter 1 and CD98 expression with triple negative breast cancer prognosis. Cancer Sci 103(2):382–389

Giaquinto AN, Sung H, Newman LA et al (2024) Breast cancer statistics 2024. CA Cancer J Clin 74(6):477–495

Häfliger P, Graff J, Rubin M et al (2018) The LAT1 inhibitor JPH203 reduces growth of thyroid carcinoma in a fully immunocompetent mouse model. J Exp Clin Cancer Res 37(1):234

Hosios AM, Hecht VC, Danai LV et al (2016) Amino acids rather than glucose account for the majority of cell mass in proliferating mammalian cells. Dev Cell 36(5):540–549

Ichinoe M, Mikami T, Yanagisawa N et al (2021) Prognostic values of L-type amino acid transporter 1 and CD98hc expression in breast cancer. J Clin Pathol 74(9):589–595

Kaira K, Takahashi T, Murakami H et al (2011) Relationship between LAT1 expression and response to platinum-based chemotherapy in non-small cell lung cancer patients with postoperative recurrence. Anticancer Res 31(11):3775–3782

Kanai Y, Segawa H, Ki M et al (1998) Expression cloning and characterization of a transporter for large neutral amino acids activated by the heavy chain of 4F2 antigen (CD98). J Biol Chem 273(37):23629–23632

Kandasamy P, Gyimesi G, Kanai Y, Hediger MA (2018) Amino acid transporters revisited: new views in health and disease. Trends Biochem Sci 43(10):752–789

Kim J, DeBerardinis RJ (2019) Mechanisms and Implications of Metabolic Heterogeneity in Cancer. Cell Metab 30(3):434–446

Koppenol WH, Bounds PL, Dang CV (2011) Otto Warburg's contributions to current concepts of cancer metabolism. Nat Rev Cancer 11(5):325–337

Leone RD, Powell JD (2020) Metabolism of immune cells in cancer. Nat Rev Cancer 20(9):516–531

Lu H, Chen I, Shimoda LA et al (2021) Chemotherapy-induced Ca2+ release stimulates breast cancer stem cell enrichment. Cell Rep 34(1):108605

Luengo A, Gui DY, Vander Heiden MG (2017) Targeting metabolism for cancer therapy. Cell Chem Biol 24(9):1161–1180

Luo X, Yin P, Reierstad S et al (2009) Progesterone and mifepristone regulate L-type amino acid transporter 2 and 4F2 heavy chain expression in uterine leiomyoma cells. J Clin Endocrinol Metab 94(11):4533–4539

Maimaiti M, Sakamoto S, Yamada Y et al (2020) Expression of L-type amino acid transporter 1 as a molecular target for prognostic and therapeutic indicators in bladder carcinoma. Sci Rep 10(1):1292

Makowski L, Chaib M, Rathmell JC (2020) Immunometabolism: from basic mechanisms to translation. Immunol Rev 295(1):5–14

Markowicz-Piasecka M, Huttunen J, Montaser A et al (2020) Hemocompatible LAT1-inhibitor can induce apoptosis in cancer cells without affecting brain amino acid homeostasis. Apoptosis 25(5–6):426–440

Martínez-Reyes I, Chandel NS (2021) Cancer metabolism: looking forward. Nat Rev Cancer 21(10):669–680

Nanda R, Chow LQ, Dees EC et al (2016) Pembrolizumab in patients with advanced triple-negative breast cancer: phase Ib KEYNOTE-012 study. J Clin Oncol 34(21):2460–2467

Okano N, Naruge D, Kawai K et al (2020) First-in-human phase I study of JPH203, an L-type amino acid transporter 1 inhibitor, in patients with advanced solid tumors. Invest New Drugs 38(5):1495–1506

Okunushi K, Furihata T, Morio H et al (2020) JPH203, a newly developed anti-cancer drug, shows a preincubation inhibitory effect on L-type amino acid transporter 1 function. J Pharmacol Sci 144(1):16–22

Rosilio C, Nebout M, Imbert V et al (2015) L-type amino-acid transporter 1 (LAT1): a therapeutic target supporting growth and survival of T-cell lymphoblastic lymphoma/T-cell acute lymphoblastic leukemia. Leukemia 29(6):1253–1266

Saito Y, Li L, Coyaud E et al (2019) LLGL2 rescues nutrient stress by promoting leucine uptake in ER+ breast cancer. Nature 569(7755):275–279

Segawa H, Fukasawa Y, Miyamoto K et al (1999) Identification and functional characterization of a Na+-independent neutral amino acid transporter with broad substrate selectivity. J Biol Chem 274(28):19745–19751

Shi L, Luo W, Huang W et al (2013) Downregulation of L-type amino acid transporter 1 expression inhibits the growth, migration and invasion of gastric cancer cells. Oncol Lett 6(1):106–112

Wang Q, Holst J (2015) L-type amino acid transport and cancer: targeting the mTORC1 pathway to inhibit neoplasia. Am J Cancer Res 5(4):1281–1294

Wang Q, Tiffen J, Bailey CG et al (2013) Targeting amino acid transport in metastatic castration-resistant prostate cancer: effects on cell cycle, cell growth, and tumor development. J Natl Cancer Inst 105(19):1463–1473

Winer EP, Lipatov O, Im SA et al (2021) Pembrolizumab versus investigator-choice chemotherapy for metastatic triple-negative breast cancer (KEYNOTE-119): a randomised, open-label, phase 3 trial. Lancet Oncol 22(4):499–511

Yao P, Xiao P, Huang Z et al (2023) Protein-level mutant p53 reporters identify druggable rare precancerous clones in noncancerous tissues. Nat Cancer 4(8):1176–1192

Yun DW, Lee SA, Park MG et al (2014) JPH203, an L-type amino acid transporter 1-selective compound, induces apoptosis of YD-38 human oral cancer cells. J Pharmacol Sci 124(2):208–217

Zhao Y, Pu C, Liu Z (2022) Essential amino acids deprivation is a potential strategy for breast cancer treatment. Breast 62:152–161

Publisher's Note Springer Nature remains neutral with regard to jurisdictional claims in published maps and institutional affiliations.